Journal Name

ARTICLE TYPE

Cite this: DOI: 10.1039/xxxxxxxxxx

Probing different spin states in xylyl radicals and ions

Mathias Steglich,[a] Andras Bodi,[a] John P. Maier,[b] and Patrick Hemberger[a]

Received Date
Accepted Date

DOI: 10.1039/xxxxxxxxxx

www.rsc.org/journalname

Resonant one-color two-photon ionization spectroscopy and mass-selected threshold photoelectron spectroscopy were applied to study the electronic doublet states of the three xylyl (methylbenzyl) radicals above 3.9 eV as well as the singlet and triplet states of the cations up to 10.5 eV. The experiments are complemented by quantum chemical calculations and Franck-Condon simulations to characterize the transitions and to identify the origin bands, allowing a precise determination of singlet-triplet splittings in the cations. Torsional motions of the methyl group notably affect the $D_0 \rightarrow D_3$ transition of *m*-xylyl. All other investigated transitions either lead to electronic states with very low rotational barriers or suffer from spectral broadening in excess of methyl torsional energy levels. The methyl internal rotational potential is faithfully reproduced with the most basic ab initio methods, yet hyperconjugation could not be identified as a significant force shaping them. Time-dependent density functional theory describes the excited electronic states better than wave function theory approaches, notably EOM-CCSD.

1 Introduction

Xylenes are used as fuel additives to improve the antiknock performance of combustion engine fuels because of their high octane ratings.[1,2] The first step upon decomposition is the formation of the resonantly stabilized xylyl radicals shown in Fig. 1, which are key species that determine the subsequent combustion processes, especially the formation and emission of harmful PAHs.[3] Several experimental studies dealt with the decomposition dynamics of these radicals on μs and ns time scales.[3–16] It was found that the closed-shell species *p*- and *o*-xylylene are directly created via H abstraction from the respective xylyl doublets, whereas *m*-xylyl rearranges to the ortho or para radical isomer prior to hydrogen elimination in model flames and microreactors.[15,17] Therefore, different synthesis routes have to be employed to generate and characterize the highly reactive diradical *m*-xylylene.[18–25] In order to understand the dynamics of the xylyl radicals, it is of fundamental interest to explore their electronically excited states, since internal energy needs to be efficiently deposited to trigger, e.g., unimolecular decomposition reactions. To this end, femtosecond laser pulses are usually applied in pump-probe experiments to explore the ultrafast evolution of electronic and vibrational energy.[26,27] Investigating electronic spectra of benzylic radicals and ions is furthermore motivated by quantum chemistry. Especially the methyl group has been shown to influence electronic spectra notably[28–31] and may act as a sensitive probe providing benchmarks for the accuracy of theoretical predictions. Methyl substitution of benzyl induces electronic state energy shifts that are different for each of the three isomers. Internal rotational minima and transition states can also relocate upon excitation or ionization, which may have a profound effect on the spectrum by affecting Franck-Condon (FC) factors even if the electronic structure changes are minimal.[32] Such phenomena can conveniently be probed by UV and photoelectron (PE) spectroscopy.

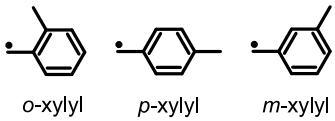

Fig. 1 Molecular structures of resonantly stabilized xylyl radicals.

Regarding spectroscopic investigations of the xylyl radicals, the literature is limited to a few studies of the first electronic transition $D_0 \rightarrow D_1$ around 2.7 eV. Vibrational frequencies and rotational constants in both electronic states were determined.[28,33–46] Very recently, these transitions were monitored by resonant two photon ionization and laser-induced fluorescence spectroscopy to investigate the interconversion of xylyl and formation of methyltropyl radicals in toluene and xylene discharge sources.[47] To study decomposition dynamics in pump-probe laser experiments, yet unexplored higher excitations need to be utilized because the energetically low-lying D_1 state cannot trigger unimolecular dissociation processes due to thermodynamic reasons. Recently, the hydrogen loss dynamics of *o*- and *p*-xylyl were investigated, albeit details on the electronic structure remained unexplored.[16] In addition, the ground states of the xylyl cations have been probed

[a] *Paul Scherrer Institute, CH-5232 Villigen-PSI, Switzerland. E-mail: mathias.steglich@psi.ch, patrick.hemberger@psi.ch*
[b] *Department of Chemistry, University of Basel, Klingelbergstrasse 80, CH-4056 Basel, Switzerland.*

by PE spectroscopy[48] and, more accurately, by threshold photoelectron (TPE) spectroscopy,[15] yielding ionization energies and vibrational frequencies. In order to understand the fast deactivation mechanisms in flames and reactors, a more profound picture of the electronic structure, including high lying excited states, has to be established if laser excitation is used to trigger chemical reactions. Motivated by these aspects, the present study describes the electronic spectra of the xylyl radicals up to 5 eV, obtained by resonant one-color two-photon ionization (R2PI). The electronic structure of the xylyl cations was explored by TPE spectroscopy up to 4 eV above the ionization energy.

2 Methods

R2PI spectroscopy

Ortho-, meta-, or para-xylene was evaporated in 5 bar helium at room temperature and discharged at the exit nozzle of a pulsed solenoid valve to produce the corresponding xylyl radicals in a supersonic jet. A molecular beam was created by skimming the supersonic expansion at 40 mm distance from the exit of the discharge source. A +300 V potential applied to the skimmer removed the ions created in the discharge before the neutral species entered the ionization region of a time-of-flight mass spectrometer. Spectral scans applying an R2PI scheme were realized by counter-propagating the radiation of an optical parametric laser (210-700 nm, $5-10$ ns, 20 Hz, 0.1 nm bandwidth) into the molecular beam. Resulting ions were extracted into a time-of-flight spectrometer and detected by a micro-channel plate. The mass-selected spectra were corrected for wavelength-dependent power variations and photon energies were calibrated with an external spectrometer ($\pm$3 meV at 4 eV). The ionization energies of the xylyl radicals are 6.94–7.11 eV.[15,48] R2PI signals can therefore be expected for photon energies above 3.47–3.56 eV.

TPE spectroscopy

TPE experiments were carried out at the photoelectron photoion coincidence (PEPICO) endstation[49] of the VUV beamline[50] at the Swiss Light Source. Synchrotron radiation was collimated, dispersed by a 150 mm^{-1} grating in grazing incidence and focussed at the exit slit, achieving an energy resolution of 5 meV at 8 eV. An MgF_2 window absorbs higher diffraction orders, and the second order free VUV beam entered the PEPICO setup. Flash vacuum pyrolysis of ortho-, meta-, or para-xylyl bromide was applied to create the xylyl radicals. The precursors were kept at 15–40°C and, together with 300 mbar Ar buffer gas, expanded through a 100 μm pinhole into a resistively heated SiC tubular reactor. The reactor temperature was optimized at up to 900°C to give a strong signal in the mass spectrum at $m/z = 105$, while minimizing the precursor signal as well as fragment peaks at lower masses. The molecular beam formed at the reactor exit was skimmed before entering the ionization region. A constant field of 250 V cm^{-1} extracted ions and electrons into the double velocity map imaging (VMI) spectrometer of the PEPICO endstation. For the photoions, both VMI and Wiley-McLaren space focussing conditions could be achieved. Threshold electrons were selected with a resolution of 5 meV from the central part of the PE image. The hot electron background was subtracted as described elsewhere.[51] Photoion mass-selected TPE spectra were acquired by scanning the photon energy in steps of 5 or 10 meV and corrected against the photon flux.

Continuous flash vacuum pyrolysis was used in the synchrotron experiments instead of discharge because of duty cycle considerations and also because the molecular beam is void of unwanted ions and electrons using this technique, which cause an unstable background in PEPICO. On the other hand, cooling of the radicals is more efficient in the pulsed discharge source because the expansion into vacuum has a higher effective backing pressure leading to more efficient supersonic jet formation.

Quantum chemical calculations

Most computations presented throughout this manuscript were obtained using the Gaussian16[52] implementation of density functional theory (DFT) and its time-dependent variant (TDDFT). The ωB97XD functional was applied in conjunction with the cc-pVTZ basis set. The numbering of electronic states is based on the state order calculated by TDDFT. FC simulations were performed with Gaussian16 and PGOPHER[53] using vibrational frequencies scaled by a factor of 0.954, as it was suggested for this DFT method.[54] For comparison, coupled cluster singles and doubles (CCSD) as well as equation-of-motion (EOM) coupled cluster calculations were carried out using Q-Chem 4.3[55] to compute ionization and excitation energies, as well as spin-flip states and electron affinities using the EOM-IP/EE/SF/EA-CCSD methods, respectively.

3 Results and Discussion

Electronic absorptions of the neutral radicals

The R2PI spectra of the neutral xylyl radicals are depicted in Fig. 2. The spectrum of benzyl recorded in the same setup and using toluene as precursor is shown for comparison. It was measured in gas phase before and further discussions can be found in the literature.[26,45,56–58] The D_1 and D_2 states of benzyl are coupled with each other via vibronic interaction (calculated oscillator strength $f_{calc}(D_1) = 3 \cdot 10^{-4}$ and $f_{calc}(D_2) = 4 \cdot 10^{-3}$). They produce some weak absorptions at 2.7-2.8 eV,[45] which is outside the R2PI detection window. The origin band of the D_3 state ($f_{calc} = 4 \cdot 10^{-2}$) at 4.062 eV and the corresponding vibrational progression up to 4.27 eV were already observed and assigned by Margraf et al.[26] in another R2PI study using a high-resolution dye laser and flash vacuum pyrolysis to generate benzyl in the gas phase. No rotational structure could be resolved due to lifetime and/or temperature-related broadening. In agreement with low-resolution studies,[56,57] the strongest vibrational excitation in D_3, the ν_5 fundamental (C–C valence mode) at 4.177 eV, is about five times weaker than the origin band, signifying little geometry change upon electronic excitation. The strong D_4 state ($f_{calc} = 0.35$) with maximum absorption at 4.89 eV appears broad, without analyzable structure, and is probably mixed with nearby Rydberg states, whose presence was suggested by complete active space (CAS) calculations.[27]

Substitution of one hydrogen on the aromatic ring by a methyl group can be seen as gentle perturbation of the electronic struc-

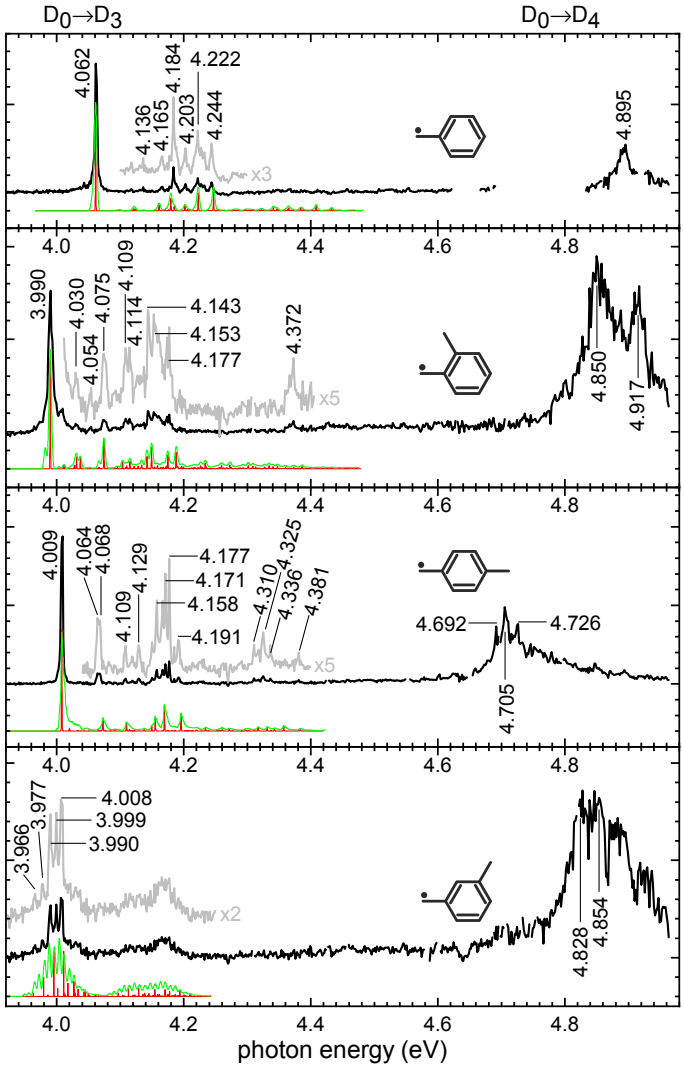

Fig. 2 R2PI spectra of xylyl radicals and benzyl (black and grey traces). Data points have been removed where strong absorptions of the precursor molecules appeared on the spectra. FC simulations of $D_0 \rightarrow D_3$ using calculated harmonic frequencies (scaled by 0.954)[54] at $T_{vib} = 0\,\mathrm{K}$ and $T_{vib} = 150\,\mathrm{K}$ are displayed in red and green, respectively.

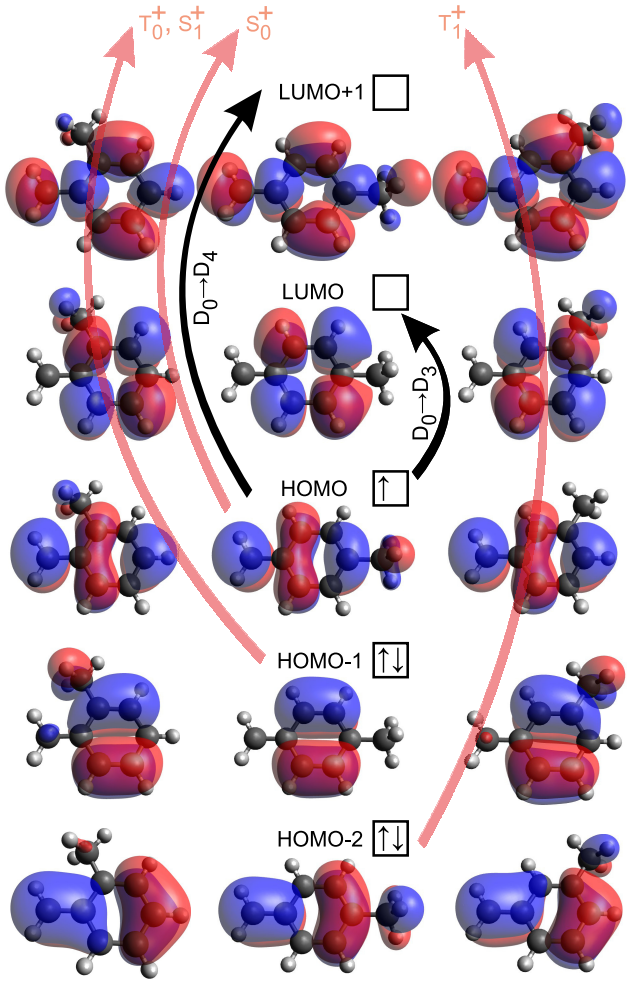

Fig. 3 Calculated molecular orbitals, occupation of the neutral radicals, and basic excitation schemes of investigated transitions.

ture. The transitions observed in this study are characterized by $\pi \rightarrow \pi^*$ electron promotion, and the main influences of the methyl group are expected to come from electrostatic interactions and electron exchange between the methyl C–H bonds and benzyl ring bond orbitals. These usually cause $\pi \rightarrow \pi^*$ excitations to redshift and transition probabilities to alter slightly. The $D_0 \rightarrow D_1$ transition of the xylyls, for example, is 37–81 meV lower in energy than in benzyl.[28,33] The $D_0 \rightarrow D_2$ origin has not been determined yet, as it is likely vibronically coupled into the D_1 state. Both transitions are calculated within <0.2 eV distance from each other with weak oscillator strengths ($f_{calc} < 6 \cdot 10^{-3}$). The excitations involved are predicted by TDDFT as mainly HOMO-1→HOMO, HOMO-2→HOMO (β electrons), with additional contributions from HOMO→LUMO, HOMO→LUMO+1 promotions (α electrons). The calculated molecular orbitals are visualized in Fig. 3.

The stronger $D_0 \rightarrow D_3$ ($f_{calc} = 0.03 - 0.05$) and $D_0 \rightarrow D_4$ ($f_{calc} = 0.3 - 0.4$) transitions, on the other hand, are characterized by simpler electron promotion schemes in the molecular orbital picture and follow HOMO→LUMO and HOMO→LUMO+1 excitations, respectively. This was confirmed by a natural transition orbital analysis as implemented in Gaussian16.[59] In both cases, the tran-

sition dipole moments are oriented in the plane of the aromatic ring (Fig. 4). The $D_0 \rightarrow D_3$ vector points perpendicular and the $D_0 \rightarrow D_4$ vector parallel to the methylene group, indicating different directions of charge density separation. The experimental redshift of the xylyl $D_0 \rightarrow D_3$ transition is 50–85 meV when compared to benzyl and is caused by stabilization of the involved orbitals upon methyl substitution. In the case of *m*-xylyl, the exact state energy, however, is not as straightforward to determine as for the other two isomers because the spectrum is void of a single strong origin band. A progression of three equally intense bands and 9 meV spacing is observed instead. Two of those bands basically coincide with the $D_0 \rightarrow D_3$ origin bands of the ortho and para isomer, but a contribution of these species to the *m*-xylyl spectrum can be excluded because the experimental conditions, especially the discharge ones, were identical in all three cases and the energy barriers to methyl migration along the ring perimeter is the same for all isomers.[15] Since the ortho and para spectra are obviously clean from spectral contamination by other isomers, the same is presumed for the meta spectrum. Consequently, we exclude isomerization of the three xylyl radicals under our experimental conditions.[47] The $D_0 \rightarrow D_3$ multiplet structure of *m*-xylyl was similarly observed in the $D_0 \rightarrow D_1$ laser induced fluorescence excitation and $D_1 \rightarrow D_0$ dispersed fluorescence spectra.[28] It can be explained by excitation of a low frequency torsional mode of the methyl group, owing to an internal rotational barrier preventing free CH_3 rotation, yet supporting only few bound states. The hindered methyl rotation in the ground and first excited state of resonance stabilized radicals has been subject of a few investigations.[28–30,37] Upon electronic excitation, the potential energy surface minimum can shift thanks to presence or absence of electronic stabilization effects, which can have a pronounced effect on the absorption spectra. For the xylyl radicals, it has been found that the torsional barrier height in the ground state is lowest in the para and highest in the ortho isomer and that they change considerably in the D_1 state.[28]

For symmetry reasons, two different methyl orientations, separated by a 60° torsional motion, are possible stationary points for the ortho and meta isomers; the in-plane C–H bond is either directed towards the methylene group or away from it. One of these orientations will be a minimum on the potential energy surface and the other a transition state. The para isomer behaves differently, since the C_s symmetry plane of the ground state is perpendicular to the aromatic ring. The two possible methyl orientations, now separated by a 30° torsional angle, are those with one C–H bond parallel or perpendicular to the aromatic ring plane. In general, bond rotation barriers are determined by a balance between orbital and electrostatic interactions.[60] However, a quantification of the different effects based on a natural bond orbital analysis,[61] as discussed further below, has proven to be largely ineffective in predicting the effects of excitation and ionization on the torsional energy surface. More qualitatively, whether or not the methyl group prefers to change its orientation upon electronic excitation may be understood by subtracting the calculated electron density in the ground state from the one in the excited state (evaluated at the ground state geometry). The thus obtained difference electron densities are plotted in Fig. 4. For the $D_0 \rightarrow D_3$

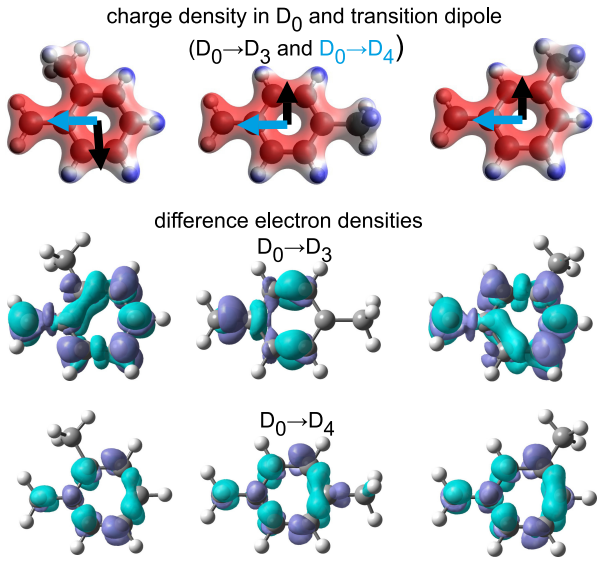

Fig. 4 Calculated D_0 charge densities of the neutral species, normalized transition dipole vectors and difference electron densities for $D_0 \rightarrow D_3$ and $D_0 \rightarrow D_4$ vertical transitions.

transition of *o*- and *m*-xylyl, an asymmetric change of electron density on the part of the aromatic ring where the methyl group is attached can be noticed, which affects the intramolecular stabilization mechanisms and potentially causes the methyl group to flip around in the excited state. No such change appears in *p*-xylyl, which is therefore predicted to keep its methyl group orientation in D_3.

A quantitative view is provided by calculating the relaxed potential energy surfaces along the $-CH_3$ torsional angle ϕ, which is plotted in Fig. 5. The curves can be approximated by cosine functions of the form $V(\phi) = E_{pot}(\cos n\phi - 1)$, with $n = 3$ for *o*-, *m*-xylyl, or $n = 6$ for *p*-xylyl. In agreement with previous qualitative predictions, the barrier to rotation E_{pot} changes its height considerably, i.e., by more than 50 meV, and its minimum coordinate by 60° when going from D_0 to D_3 in the ortho and meta isomers. In contrast, *p*-xylyl keeps the $-CH_3$ orientation (structure c) and is essentially a free rotor since the corresponding PE surfaces are shallow (<1 meV).

To characterize the $D_0 \rightarrow D_3$ transition in more detail, FC simulations using calculated geometries and scaled harmonic frequencies were carried out as displayed as red traces in Fig 2. For *o*-xylyl, excitations of the –CH_3 torsional mode $\nu_{44}(a'')$ had to be suppressed to achieve good agreement with the experimental data, because no low-energy progression attributable to such vibration is present in the measured spectrum. The corresponding calculated potential energy surface in D_3 is rather flat (16 meV; Fig. 5) and, at the anharmonic level,[62] not even the fundamental of $\nu_{44}(a'')$ fits in the potential well. No transition into localized torsional levels can be observed as the methyl group is essentially a free rotor and contributions to the spectrum can thus be excluded. The strong band at 3.99 eV is therefore assigned as the origin transition. The weak vibronic structure up to 4.2 eV is due to single excitations of totally symmetric in-plane C–C bending/stretching and C–H bending modes account-

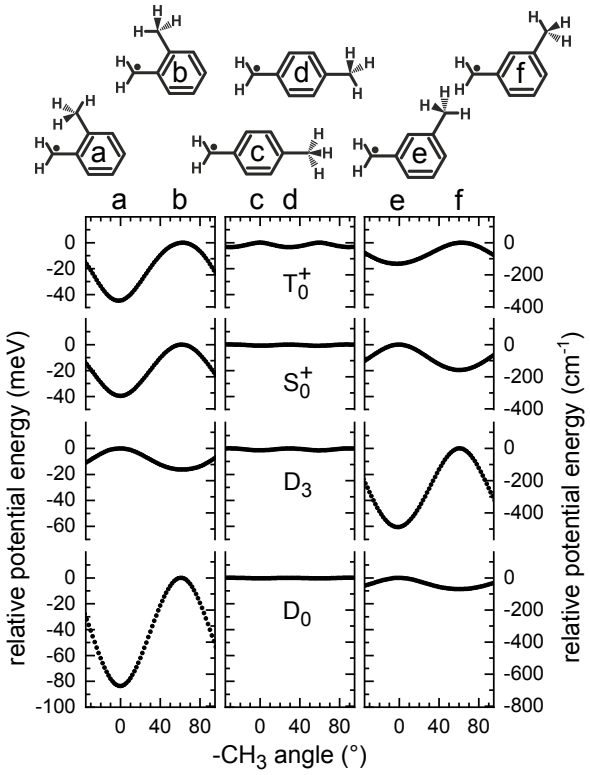

Fig. 5 Calculated potential energy surfaces for rotation of the methyl group in different electronic states of xylyl radicals and cations.

ing for the structural relaxation in D_3. Near the origin, weak hot and sequence bands involving out-of-plane C–C bendings might contribute, causing additional broadening of this band. Similar modes are calculated to determine the $D_0 \rightarrow D_3$ progressions of *p*- and *m*-xylyl. The latter one, however, features further structure around the origin caused by excitations of the $-CH_3$ torsional mode $\nu_{45}(a'')$. Harmonic and anharmonic frequency calculations were unable to predict vibrational energies in good agreement with the observed spacing of this structure, which is not surprising considering the cosine shaped potential energy curves of Fig. 5 and the high electronic excitation (D_3), which is even difficult to describe using state-of-the-art EOM and CIS calculations (see below). The origin band is modelled to correspond to the first resolved resonance in the spectrum, but since hot bands can contribute with similar intensity, an assignment to either the 3.966 eV or the 3.977 eV band is tentative at the moment. More insights may be gained by applying narrow-band dye lasers.

FC simulations of the $D_0 \rightarrow D_4$ transition were not attempted due to the broad and largely unstructured appearance in all three isomers. In *p*-xylyl, three peaks with ≈ 17 meV spacing are observed, that cannot be attributed with confidence to any vibration in D_4. Contributions from other electronic states, e .g., via vibronic coupling, are possible, similarly to the case of benzyl.[27] Such intermediate level structure can also take part in the broadening of the ortho and meta spectra, which may additionally be affected by more complex structural relaxations in D_4, including an out-of-plane deformation of the methylene group, as suggested by TDDFT optimizations.

Performance of TDDFT, CIS, and EOM-CCSD

The electronic structure of the benzyl radical was studied by Werner Bingel in 1955, who proposed the ordering of the electronic states as $D_0(^2B_2)$, $D_1(^2A_2)$, $D_2(^2B_2)$, $D_3(^2A_2)$, and $D_4(^2B_2)$.[63] Although Johnson and Albrecht suggested a slightly different ordering of B_2, B_2, ?, B_2, and A_2 based on a three-step photoselection experiment 13 years later,[64] the Bingel ordering has generally been accepted since,[26] notwithstanding the exact nature of the close-lying D_1 and D_2 states. Tonokura and Koshi used TDDFT calculations with a double-ζ basis set and confirmed Bingel's results even if the B_1 and B_2 symmetries are exchanged in their work due to their choice of principal plane,[45] an apparently recurring source of confusion in the study of C_{2v} species. Recently, Röder et al. applied cutting-edge wave function theory methods, among them EOM-EE-CCSD and CASSCF(7,11)+MRCI calculations using a double-ζ basis set augmented with s and p Rydberg orbitals, and arrived at a significantly different ordering of B_2, B_2, A_2, A_1, A_1, with the totally symmetric D_3 and D_4 states having strong Rydberg state character.[27] Methyl substitution in benzyl reduces the symmetry to C_s and only perturbs the electronic structure slightly, which means that electronic structure insights into one species may be relevant for the other, as well. The fact that the Franck-Condon simulation reproduces the fine structure of the xylyl D_3 states in a satisfactory manner indicates that the underlying TDDFT results are reliable. In line with the HOMO-2 to LUMO$+1$ orbitals all being of a" symmetry (*o*- and *m*-xylyl; see Fig. 3), TDDFT predicts that at least the first five electronic states are of A" symmetry, and the D_3 state in benzyl is of A_2 symmetry, corroborating Bingel's original semi-empirical calculations. Although the standard cc-pVTZ basis set lacks diffuse or Rydberg-type basis functions, it was sufficient for the FC simulations. While there could be Rydberg states in this energy range, which cannot be described without such diffuse functions, this suggests that the spectroscopically observed D_3 state is not one of them.

In addition to TDDFT calculations, we have applied wave function theory, i.e., configuration interaction singlets (CIS) and various equation-of-motion coupled cluster singles and doubles (EOM-CCSD) approaches, using the cc-pVTZ basis set. In the electron affinity (EA), ionization potential (IP), excitation energy (EE), and spin-flip (SF) EOM calculations, the singlet cation, singlet anion, doublet radical, and quartet radical states, respectively, were used as reference at the optimized D_0 geometry. The vertical excitation energies were referenced to the doublet radical energy to obtain the energy levels shown in Fig. 6. CIS excitation energies are all above 5.5 eV and are not plotted, which also confirms that singly excited Hartree-Fock determinants describe the excited electronic states very poorly. EOM-IP-CCSD and EOM-EA-CCSD calculations suffer from ‚ferocious' orbital relaxation associated with the removal or addition of an electron as well as the absence of triples corrections to account for electron excitation in concert with, e.g., electron addition in the case of EOM-EA-CCSD.[65] The excited state energies are, thus, severely overestimated, and the xylyl D_3 state, i.e., 4 A", is predicted at 6.4 and 7.7 eV using EOM-EA-CCSD and EOM-IP-CCSD, respectively.

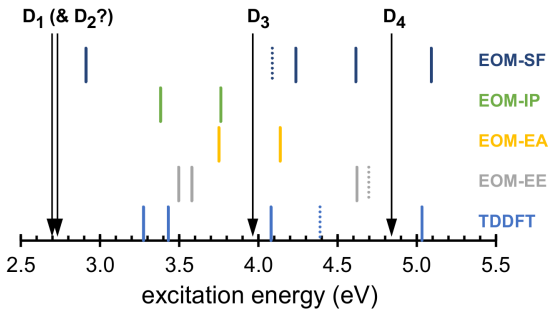

Fig. 6 Computed vertical excitation energies in *o*-xylyl at different levels of theory using the cc-pVTZ basis set. Arrows indicate observed transitions (origin bands) and dotted lines indicate computed quartet ground state energies.

The failure of EOM-SF-CCSD to even qualitatively reproduce the energy levels may be related to the inadequacy of the quartet reference wave function to describe these states. While the doublet Hartree-Fock wave function is also affected by considerable spin contamination ($< S^2 >= 1.39$), which may compromise wave function theory approaches that use it as a reference, the EOM-EE-CCSD excitation energies at least qualitatively reproduce the experimentally observed level spacings, albeit still overestimating the excitation energies more than TDDFT. Because the D_3 and Q_0 (ground state quartet) states are both of A" symmetry and rather close in energy in the xylyl radical, complicating their separation based on symmetry, whereas they are of $^2A_2$ and $^2B_2$ symmetry in the benzyl radical, respectively, we have optimized the D_3 state of benzyl using EOM-EE-CCSD/cc-pVDZ. The resulting FC simulation is almost identical to the one obtained from ωB97XD/cc-pVTZ (Fig. 2), confirming the identity of the EOM-EE-CCSD D_3 state, although the calculated excitation energy is more than 0.6 eV higher than experimentally observed.

Electronic states of the cations

The TPE spectra for ionization into the ionic ground state[15] ($D_0 \rightarrow S_0^+$) are shown along with energetically higher transitions up to 10.5 eV in Fig. 7. Assignments of the main spectral features to the two singlet (S_0^+, S_1^+) and two triplet states (T_0^+, T_1^+) are based on DFT and TDDFT energies. The subtracted electron densities for the vertical $D_0 \rightarrow S_0^+$ and $D_0 \rightarrow T_0^+$ ionization processes in Fig. 8 are straightforward to interpret as they resemble the squared molecular orbitals of Fig. 3 from which ionization took place, i.e., Koopmans' theorem holds. In case of S_0^+, ionization is caused by removal of the single HOMO electron, while ionization from HOMO-1 gives rise to the lowest triplet state. The first excited singlet state S_1^+ is also derived by electron removal from HOMO-1, but with total spin $S = 0$ as a result, whereas ionization from HOMO-2 gives rise to the T_1^+ state.

FC simulations at 0 K (red trace) and 400 K (green trace) vibrational temperature have been realized to identify the origin bands and strongest vibrational excitations. The singlet and triplet ground states feature strong and isolated origin bands, from which accurate ionization energies and singlet-triplet splittings can be derived. The former were given before as $E_{ion}^{ortho} = (7.08 \pm 0.01)$ eV, $E_{ion}^{para} = (6.94 \pm 0.01)$ eV, $E_{ion}^{meta} = (7.11 \pm 0.01)$ eV,[15] while

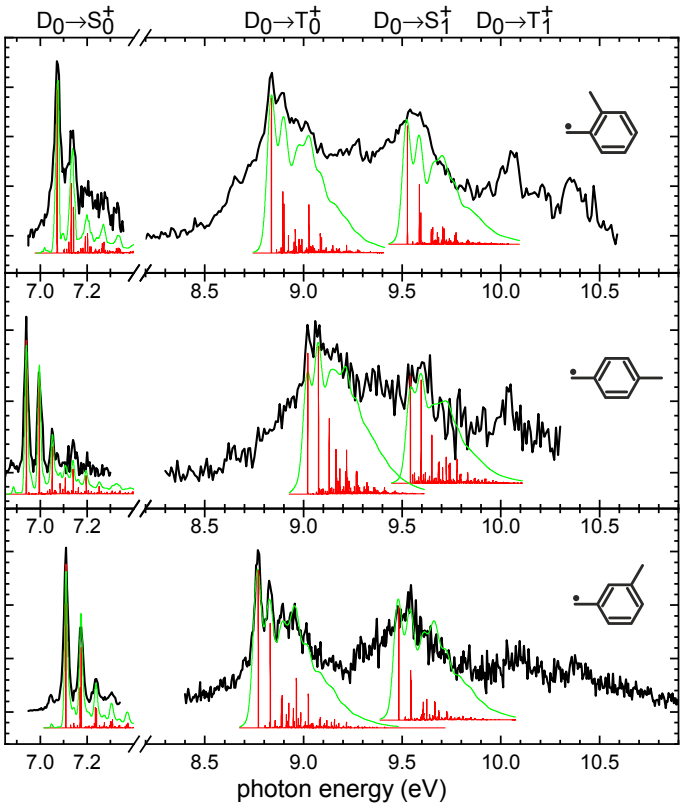

Fig. 7 TPE spectra of the xylyl radicals. FC simulations at $T_{vib} = 0$ K are displayed in red and at $T_{vib} = 400$ K in green. Note the slightly different energy scales for S_0^+ and T_0^+.

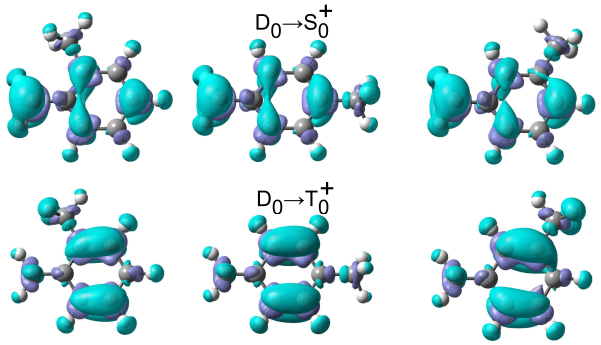

Fig. 8 Calculated difference electron densities for $D_0 \rightarrow S_0^+$ and $D_0 \rightarrow T_0^+$ vertical ionization.

the latter are determined herein as $\Delta E^{ortho}_{T_0-S_0} = (1.76 \pm 0.02)$ eV, $\Delta E^{para}_{T_0-S_0} = (2.08 \pm 0.02)$ eV, and $\Delta E^{meta}_{T_0-S_0} = (1.66 \pm 0.02)$ eV, respectively. For comparison, the corresponding values of benzyl were measured[66] as $E_{ion} = 7.252$ eV, $\Delta E_{T_0-S_0} = 1.928$ eV. The addition of the methyl group apparently causes a lowering of the singlet and triplet ground state energies in the xylyl cations. Although the singlet-triplet gaps of the ortho and meta isomers are also lowered, the highest $\Delta E_{T_0-S_0}$ value can be found in *p*-xylyl. Following Koopmans' theorem, this may be traced back to the energy difference between the HOMO and HOMO-1 molecular orbitals (Fig. 3), which is found with DFT to be largest in the para isomer; the HOMO-1 is about 0.2 eV lower and the HOMO 0.1 eV higher in energy when compared to the other two isomers. The higher HOMO-1 electron bonding energy in *p*-xylyl is graphically explained by the fact that, in general, the energy of a molecular orbital decreases as the number of nodes decrease (2 for meta and ortho vs. 1 node for para), which leads to a more efficient electron delocalization on the aromatic ring (and vice versa for the HOMO). This energy difference can be recovered in the different $D_0 \rightarrow D_1$ transition energies of the neutrals,[28] which, as mentioned before, are partly described by HOMO-1→HOMO electron promotion.

The vibrational excitations within the S_0^+ structure can be associated with in-plane C–C ring deformation and in-plane C–H bending motions. As can be seen in Fig. 5, the orientation of the methyl group in all three isomers is predicted to be the same as in the neutral ground states. Progressions from $-CH_3$ torsional vibrations are therefore not to be expected in the $D_0 \rightarrow S_0^+$ TPE spectra. In the T_0^+ state of *p*- and *m*-xylyl, the fully relaxed structures (d,e) are those with the methyl group rotated by 30° and 60°, respectively, compared to D_0. However, spectral broadening prevents the corresponding low-energy progressions from being resolved. Instead, the main observable vibrational features are similar to those in S_0^+ and are composed of in-plane ring deformation and C–H bending modes. The comparatively strong PE intensity on the red tail of the T_0^+ origin bands is not accounted for by the FC simulations, and can probably be explained by hot bands and autoionization resonances. This applies also to the first excited singlet state, which appears broad and without discernible vibrational structure in all three isomers. The FC simulations are merely plotted to distinguish the S_1^+ state at 9.5–9.6 eV from the T_1^+ state at 10.0–10.1 eV. The broadening, which is probably explained by short excited state lifetimes, hampers a precise location of the origin bands.

Role of hyperconjugation in the methyl rotor barrier

We have evaluated the ionization energies and methyl internal rotational barriers at six levels of theory for the three xylyl isomers computing the neutral doublet and the ionic singlet and triplet ground states, namely at the (U)HF/6-31G(d), (RO)HF/6-31G(d), ωB97X-D/cc-pVTZ, CCSD/cc-pVTZ//CCSD/cc-pVDZ, CBS-QB3, and G4 levels of theory. When comparing the results for the ionization energies between different levels of theory, the hierarchy of quantum chemical approaches becomes evident. Restricted and unrectricted Hartree-Fock ionization energies disagree with each other and also with the other methods most. DFT and CCSD methods agree quite well with each other and approach the composite method results. Finally, G4 and CBS-QB3 ionization energies are practically indistinguishable. However, when rotational barriers are compared, even the most basic (RO/U)HF/6-31G(d) calculation reproduces them well, and the hierarchy of quantum chemical approaches disappears. This leads us to conclude that the methyl rotational barriers are the result of interactions that are easy to calculate with the most basic quantum chemical approaches, even without electron correlation. One potential driving force could be hyperconjugation, previously proposed to play a determining role in similar internal rotational barriers.[29,30]

Concepts such as hyperconjugation or steric hindrance are often applied to explain bond rotational barriers. A recent theoretical assessment of small non-aromatic compounds suggests that it is in fact the electrostatic interaction that mainly determines the barrier heights.[60] However, all these interactions have their fundamental origin in the electron density of the system and are often difficult to disentangle from each other. The xylyl radicals show markedly different methyl group rotational barriers in the various electronic states. Here, we used a natural bond analysis (NBO v.3.1[61] implemented in Gaussian16) to obtain the energies from quantummechanical donor/acceptor interactions between the methyl group and the benzyl ring in the two possible methyl group positions for each isomer and electronic state. It is found that the main contribution to this hyperconjugation comes from filled C–H bond orbitals of the methyl group donating part of their occupation into empty C–C bond orbitals on the nearby part of the benzyl ring. The summed magnitude of these exchange energies $\sum_i E^i_{xc}$ depends on the methyl orientation. The difference between the minimum and maximum energy structure $\Delta E_h = \sum_i^{min} E^i_{xc} - \sum_i^{max} E^i_{xc}$ then contributes to the rotational barrier E_{pot}. If we neglect effects from steric hindrance, the potential well depth is basically the sum of the hyperconjugation energy difference and contributions from electrostatic interactions $E_{pot} = \Delta E_h + \Delta E_e$. The calculated values of E_{pot} and ΔE_h are compared with each other in Table 1. In the ground state of *o*-xylyl, for example, hyperconjugation favors the methyl position a over b (Fig. 5) by 176 meV, whereas the total rotation barrier is only 84 meV deep, i.e., the electrostatic interactions are such that structure b is preferred. In all states of *p*-xylyl, ΔE_h and ΔE_e basically balance each other, resulting in almost flat PE surfaces. On the other hand, hyperconjugation favors the saddle points (negative ΔE_h values) of the methyl torsional potential energy surface for *p*-xylyl in D_0 and S_0^+, for *m*-xylyl in D_0, and for *o*-xylyl in the S_0^+ and T_0^+ states. These findings indicate that hyperconjugation cannot be singled out as responsible for the stabilization/destabilization of the methyl conformers and, thus, for the depth of the potential well. As indicated in the literature, the latter involves effects of electrostatic, steric, kinetic and exchange correlation, as well as Fermionic quantum contributions, which contribute differently as the chemical bond rotates. While in the case of 5-methyl-2-furanyl-methyl and α-methylbenzyl radicals[29,30] hyperconjugative effects seem to mirror the stability of the methyl conformation in the ground and excited state, it is the

Table 1 Calculated methyl rotor potentials E_{pot} in comparison to methyl group – benzyl ring hyperconjugation energy difference ΔE_h (values in meV).

	o-xylyl		*p*-xylyl		*m*-xylyl	
state	E_{pot}	ΔE_h	E_{pot}	ΔE_h	E_{pot}	ΔE_h
D_0	84	176	<1	-23	9	-75
D_3	16	–	1	–	61	–
S_0^+	40	-8	<1	-16	20	33
T_0^+	45	-23	3	108	16	102

Table 2 Experimental electronic state energies (origin band positions) of xylyl and benzyl radicals in eV (lit. values in parentheses)

state	benzyl	*o*-xylyl	*p*-xylyl	*m*-xylyl
D_1	(2.728) [45]	(2.647) [28,33]	(2.691) [28,33]	(2.662) [28,33]
D_3	4.062±0.003	3.990±0.003	4.009±0.003	3.977±0.012
D_4	$4.89^{+0.01}_{-0.02}$	$4.85^{+0.01}_{-0.07}$	$4.692^{+0.005}_{-0.030}$	$4.82^{+0.01}_{-0.06}$
S_0^+	(7.252) [66]	7.08±0.01	6.94±0.01	7.11±0.01
T_0^+	(9.180) [66]	8.84±0.01	9.02±0.01	8.77±0.01
S_1^+	(9.62) [66]	$9.53^{+0.02}_{-0.10}$	9.54±0.01	$9.48^{+0.07}_{-0.20}$
T_1^+	–	$10.05^{+0.02}_{-0.10}$	$10.04^{+0.02}_{-0.10}$	$10.09^{+0.02}_{-0.10}$

balance of all mentioned effects that determine the orientation of the methyl group in the xylyl radicals and ions.

4 Summary

The strong electronic absorptions of the xylyl radicals between 3.9 and 5 eV have been explored by R2PI and characterized using quantumchemical calculations. The $D_0 \rightarrow D_3$ and $D_0 \rightarrow D_4$ excitations are redshifted compared to those in benzyl. Torsional vibrations of the methyl group were observed to affect the $D_0 \rightarrow D_3$ origin of *m*-xylyl, which is split into three almost equally intense bands with 9 meV spacing. The two lowest singlet and triplet states of the xylyl cations were probed by TPE spectroscopy up to 10.5 eV. The measured state energies of the neutrals and cations are summarized in Table 2. All transitions are characterized by promotions of π electrons from the aromatic ring. Vibronic bands observed in the spectra originate therefore mainly from excitations of in-plane ring deformation modes. Calculated rotation barriers of the methyl group are different in each isomer and electronic state. While the respective PE surface is basically flat in all states of *p*-xylyl, it depends heavily on the specific electronic excitation in the ortho and meta isomers. Intramolecular donor-acceptor electron exchange competes with electrostatic repulsion to form the potential well for torsional motions of the methyl group. Surprisingly, all tested flavors of EOM-CCSD calculations compared worse with experimental electronic excited state energies than TD-DFT methods. On the other hand, the rotational barriers were well reproduced by even the most rudimentary Hartree-Fock ground state calculations, and correlated poorly with changing hyperconjugation contributions, which suggests that singling out hyperconjugation as the driving force for conformational change may be questionable unless validated on a suitably large set of conformers.

Acknowledgement

This project was funded by the Swiss Federal Office of Energy (SFOE, Contract Number SI/501269-01) and by the Laboratory for Thermal Processes and Combustion (LTV) at the Paul Scherrer Institute. The PEPICO experiments were carried out at the VUV beamline of the Swiss Light Source.

References

1 D. Gregory, R. A. Jackson and P. J. Bennett, *Combustion and Flame*, 1999, **118**, 459–468.

2 R. da Silva, R. Cataluna, E. W. de Menezes, D. Samios and C. M. S. Piatnicki, *Fuel*, 2005, **84**, 951–959.

3 C. Cavallotti, M. Derudi and R. Rota, *Proc. Combust. Inst.*, 2009, **32**, 115–121.

4 O. L. Chapman, J. W. Johnson, R. J. McMahon and P. R. West, *J. Am. Chem. Soc.*, 1988, **110**, 501–509.

5 I. D. Costa, R. A. Eng, A. Gebert and H. Hippler, *Proc. Comb. Inst.*, 2000, **28**, 1537–1543.

6 R. X. Fernandes, A. Gebert and H. Hippler, *Proc. Comb. Inst.*, 2002, **29**, 1337–1343.

7 N. Hansen, T. Kasper, S. J. Klippenstein, P. R. Westmoreland, M. E. Law, C. A. Taatjes, K. Kohse-Höinghaus, J. Wang and T. A. Cool, *J. Phys. Chem. A*, 2007, **111**, 4081–4092.

8 G. da Silva and J. W. Bozzelli, *J. Phys. Chem. A*, 2009, **113**, 12045–12048.

9 G. da Silva, J. A. Cole and J. W. Bozzelli, *J. Phys. Chem. A*, 2009, **113**, 6111–6120.

10 G. da Silva, E. E. Moore and J. W. Bozzelli, *J. Phys. Chem. A*, 2009, **113**, 10264–10278.

11 Y. Li, L. Zhang, Z. Tian, T. Yuan, J. Wang, B. Yang and F. Qi, *Energy Fuels*, 2009, **23**, 1473–1485.

12 T. Zhang, L. Zhang, X. Hong, K. Zhang, F. Qi, C. K. Law, T. Ye, P. Zhao and Y. Chen, *Combust. Flame*, 2009, **156**, 2071–2083.

13 M. Steinbauer, P. Hemberger, I. Fischer and A. Bodi, *ChemPhysChem*, 2011, **12**, 1795–1797.

14 P. Hemberger, A. J. Trevitt, E. Ross and G. da Silva, *J. Phys. Chem. Lett.*, 2013, **4**, 2546–2550.

15 P. Hemberger, A. J. Trevitt, T. Gerber, E. Ross and G. daSilva, *J. Phys. Chem. A*, 2014, **118**, 3593–3604.

16 K. Pachner, M. Steglich, P. Hemberger and I. Fischer, *J. Chem. Phys.*, 2017, **147**, 084303/1–084303/9.

17 T. Bierkandt, P. Hemberger, P. Osswald, M. Kohler and T. Kasper, *Proc. Combust. Inst.*, 2017, **36**, 1223–1232.

18 E. Migirdicyan and J. Baudet, *J. Am. Chem. Soc.*, 1975, **97**, 7400–7404.

19 S. K. Pollack, B. C. Raine and W. J. Hehre, *J. Am. Chem. Soc.*, 1981, **103**, 6308–6313.

20 B. B. Wright and M. S. Platz, *J. Am. Chem. Soc.*, 1983, **105**, 628–630.

21 P. G. Wenthold, J. B. Kim and W. C. Lineberger, *J. Am. Chem.*

Soc., 1997, **119**, 1354–1359.
22 L. A. Hammad and P. G. Wenthold, *J. Am. Chem. Soc.*, 2000, **122**, 11203–11211.
23 P. Neuhaus, D. Grote and W. Sander, *J. Am. Chem. Soc.*, 2008, **130**, 2993–3000.
24 W. C. Lineberger and T. Borden, *Phys. Chem. Chem. Phys.*, 2011, **13**, 11792–11813.
25 M. Steglich, V. B. F. Custodis, A. J. Trevitt, G. daSilva, A. Bodi and P. Hemberger, *J. Am. Chem. Soc.*, 2017, **139**, 14348–14351.
26 M. Margraf, B. Noller, C. Schröter, T. Schultz and I. Fischer, *J. Chem. Phys.*, 2010, **133**, 074304/1–074304/5.
27 A. Röder, A. Humeniuk, J. Giegerich, I. Fischer, L. Poisson and R. Mitrić, *Phys. Chem. Chem. Phys.*, 2017, **19**, 12365–12374.
28 T.-Y. D. Lin and T. A. Miller, *J. Phys. Chem.*, 1990, **94**, 3554–3559.
29 N. M. Kidwell, N. J. Reilly, B. Nebgen, D. N. Mehta-Hurt, R. D. H. amd D. L. Kokkin, M. C. McCarthy, L. V. Slipchenko and T. S. Zwier, *J. Phys. Chem. A*, 2013, **117**, 13465–13480.
30 N. M. Kidwell, D. N. Mehta-Hurt, J. A. Korn and T. S. Zwier, *J. Phys. Chem. A*, 2016, **120**, 6434–6443.
31 D. Kim, K. Y. Yang, H. M. Kim, T.-R. Kim, N. J. Kim, S. Shin and S. K. Kim, *Phys. Chem. Chem. Phys.*, 2017, **19**, 22375–22384.
32 F. Holzmeiera, M.-P. Herbert, I. Fischer, M. Steglich, A. Bodi and P. Hemberger, *J. Anal. Appl. Pyrolysis*, 2017, **124**, 454–460.
33 T. R. Charlton and B. A. Thrush, *Chem. Phys. Lett.*, 1986, **125**, 548–553.
34 K. Tokumura, M. Udagawa, T. Ozaki and M. Itoh, *Chem. Phys. Lett.*, 1987, **141**, 558–563.
35 C. Cossart-Magos and D. Cossart, *Mol. Phys.*, 1988, **65**, 627–647.
36 M. Fukushima and K. Obi, *J. Chem. Phys.*, 1990, **93**, 8488–8497.
37 T.-Y. D. Lin, X.-Q. Tan, T. M. Cerny, J. M. Williamson, D. W. Cullin and T. A. Miller, *Chem. Phys.*, 1992, **167**, 203–214.
38 M. Fujiwara and Y. Tanimoto, *J. Phys. Chem.*, 1994, **98**, 5695–5700.
39 J. I. Selco and P. G. Carrick, *J. Mol. Spectrosc.*, 1995, **173**, 277–295.
40 I. S. Choi and S. K. Lee, *Bull. Korean Chem. Soc.*, 1995, **16**, 281–284.
41 I. S. Choi and S. K. Lee, *Bull. Korean Chem. Soc.*, 1995, **16**, 1089–1093.
42 I. S. Choi and S. K. Lee, *Bull. Korean Chem. Soc.*, 1996, **17**, 749–753.
43 M. H. Suh, S. K. Lee and T. A. Miller, *J. Mol. Spectrosc.*, 1999, **194**, 211–218.
44 S. K. Lee and S. Y. Chae, *Chem. Phys.*, 2002, **284**, 625–631.
45 K. Tonokura and M. Koshi, *J. Phys. Chem. A*, 2003, **107**, 4457–4461.
46 A. Matsugi and A. Miyoshi, *Chem. Phys. Lett.*, 2012, **521**, 26–30.
47 N. Reilly, G. daSilva, C. M. Wilcox, Z. Ge, D. L. Kokkin, T. P. Troy, K. Nauta, S. H. Kable, M. C. McCarthy and T. W. Schmidt, *J. Phys. Chem. A*, 2018, **122**, 1261–1269.
48 K. Hayashibara, G. H. Kruppa and J. L. Beauchamp, *J. Am. Chem. Soc.*, 1986, **108**, 5441–5443.
49 B. Sztáray, K. Voronova, K. G. Torma, K. J. Covert, A. Bodi, P. Hemberger, T. Gerber and D. L. Osborn, *J. Chem. Phys.*, 2017, **147**, 013944/1–013944/10.
50 M. Johnson, A. Bodi, L. Schulz and T. Gerber, *Nucl. Instrum. Methods Phys. Res. A*, 2009, **610**, 597–603.
51 B. Sztáray and T. Baer, *Rev. Sci. Instrum.*, 2003, **74**, 3763–3768.
52 M. J. Frisch, G. W. Trucks, H. B. Schlegel, G. E. Scuseria, M. A. Robb, J. R. Cheeseman, G. Scalmani, V. Barone, G. A. Petersson, H. Nakatsuji, X. Li, M. Caricato, A. V. Marenich, J. B. B. G. Janesko, R. Gomperts, B. Mennucci, H. P. Hratchian, J. V. Ortiz, A. F. Izmaylov, J. L. Sonnenberg, D. Williams-Young, F. Ding, F. Lipparini, F. Egidi, J. Goings, B. Peng, A. Petrone, T. Henderson, D. Ranasinghe, V. G. Zakrzewski, J. Gao, N. Rega, G. Zheng, W. Liang, M. Hada, M. Ehara, K. Toyota, R. Fukuda, J. Hasegawa, M. Ishida, T. Nakajima, Y. Honda, O. Kitao, H. Nakai, T. Vreven, K. Throssell, J. A. Montgomery, Jr., J. E. Peralta, F. Ogliaro, M. J. Bearpark, J. J. Heyd, E. N. Brothers, K. N. Kudin, V. N. Staroverov, T. A. Keith, R. Kobayashi, J. Normand, K. Raghavachari, A. P. Rendell, J. C. Burant, S. S. Iyengar, J. Tomasi, M. Cossi, J. M. Millam, M. Klene, C. Adamo, R. Cammi, J. W. Ochterski, R. L. Martin, K. Morokuma, O. Farkas, J. B. Foresman, and D. J. Fox, *Gaussian 16, Revision A.03*, Wallingford, ct: Gaussian, inc. technical report, 2016.
53 C. M. Western, *J. Quant. Spectrosc. Radiat. Transfer*, 2016, **186**, 221–242.
54 M. K. Kesharwani, B. Brauer and J. M. L. Martin, *J. Phys. Chem. A*, 2015, **119**, 1701–1714.
55 Y. Shao, Z. Gan, E. Epifanovsky, A. T. Gilbert, M. Wormit, J. Kussmann, A. W. Lange, A. Behn, J. Deng, X. Feng, D. Ghosh, M. Goldey, P. R. Horn, L. D. Jacobson, I. Kaliman, R. Z. Khaliullin, T. Kuś, A. Landau, J. Liu, E. I. Proynov, Y. M. Rhee, R. M. Richard, M. A. Rohrdanz, R. P. Steele, E. J. Sundstrom, H. L. W. III, P. M. Zimmerman, D. Zuev, B. Albrecht, E. Alguire, B. Austin, G. J. O. Beran, Y. A. Bernard, E. Berquist, K. Brandhorst, K. B. Bravaya, S. T. Brown, D. Casanova, C.-M. Chang, Y. Chen, S. H. Chien, K. D. Closser, D. L. Crittenden, M. Diedenhofen, R. A. D. Jr., H. Do, A. D. Dutoi, R. G. Edgar, S. Fatehi, L. Fusti-Molnar, A. Ghysels, A. Golubeva-Zadorozhnaya, J. Gomes, M. W. Hanson-Heine, P. H. Harbach, A. W. Hauser, E. G. Hohenstein, Z. C. Holden, T.-C. Jagau, H. Ji, B. Kaduk, K. Khistyaev, J. Kim, J. Kim, R. A. King, P. Klunzinger, D. Kosenkov, T. Kowalczyk, C. M. Krauter, K. U. Lao, A. D. Laurent, K. V. Lawler, S. V. Levchenko, C. Y. Lin, F. Liu, E. Livshits, R. C. Lochan, A. Luenser, P. Manohar, S. F. Manzer, S.-P. Mao, N. Mardirossian, A. V. Marenich, S. A. Maurer, N. J. Mayhall, E. Neuscamman, C. M. Oana, R. Olivares-Amaya, D. P. O'Neill, J. A. Parkhill, T. M. Perrine, R. Peverati, A. Prociuk, D. R. Rehn, E. Rosta, N. J. Russ, S. M.

Sharada, S. Sharma, D. W. Small, A. Sodt, T. Stein, D. Stück, Y.-C. Su, A. J. Thom, T. Tsuchimochi, V. Vanovschi, L. Vogt, O. Vydrov, T. Wang, M. A. Watson, J. Wenzel, A. White, C. F. Williams, J. Yang, S. Yeganeh, S. R. Yost, Z.-Q. You, I. Y. Zhang, X. Zhang, Y. Zhao, B. R. Brooks, G. K. Chan, D. M. Chipman, C. J. Cramer, W. A. G. III, M. S. Gordon, W. J. Hehre, A. Klamt, H. F. S. III, M. W. Schmidt, C. D. Sherrill, D. G. Truhlar, A. Warshel, X. Xu, A. Aspuru-Guzik, R. Baer, A. T. Bell, N. A. Besley, J.-D. Chai, A. Dreuw, B. D. Dunietz, T. R. Furlani, S. R. Gwaltney, C.-P. Hsu, Y. Jung, J. Kong, D. S. Lambrecht, W. Liang, C. Ochsenfeld, V. A. Rassolov, L. V. Slipchenko, J. E. Subotnik, T. V. Voorhis, J. M. Herbert, A. I. Krylov, P. M. Gill and M. Head-Gordon, *Molecular Physics*, 2015, **113**, 184–215.

56 N. Ikeda, N. Nakashima and K. Yoshihara, *J. Phys. Chem.*, 1984, **88**, 5803–5806.

57 F. Markect and P. Pagsberg, *Chem. Phys. Lett.*, 1993, **209**, 445–454.

58 Y. Song, X. Zheng, M. Lucas and J. Zhang, *Phys. Chem. Chem. Phys.*, 2011, **13**, 8296–8305.

59 R. L. Martin, *J. Chem. Phys.*, 2003, **118**, 4775–4777.

60 S. B. Liu, *J. Phys. Chem. A*, 2013, **117**, 962–965.

61 A. E. Reed, L. A. Curtiss and F. Weinhold, *Chem. Rev.*, 1988, **88**, 899–926.

62 V. Barone, *J. Chem. Phys.*, 2005, **122**, 1–10.

63 W. Bingel, *Z. Naturforschg.*, 1955, **10a**, 462–476.

64 P. M. Johnson and A. C. Albrecht, *J. Chem. Phys.*, 1968, **48**, 851–865.

65 P. U. Manohar, J. F. Stanton and A. I. Krylov, *J. Chem. Phys.*, 2009, **131**, 114112/1–114112/13.

66 J. D. Savee, J. Zádor, P. Hemberger, B. Sztáray, A. Bodi and D. L. Osborn, *Mol. Phys.*, 2015, **113**, 2217–2227.